Multiscale Medial Shape-Based Analysis of Image Objects

STEPHEN M. PIZER, SENIOR MEMBER, IEEE, GUIDO GERIG, MEMBER, IEEE, SARANG JOSHI, AND STEPHEN R. AYLWARD, ASSOCIATE MEMBER, IEEE

Invited Paper

Medial representation of a three-dimensional (3-D) object or an ensemble of 3-D objects involves capturing the object interior as a locus of medial atoms, each atom being two vectors of equal length joined at the tail at the medial point. Medial representation has a variety of beneficial properties, among the most important of which are 1) its inherent geometry, provides an object-intrinsic coordinate system and thus provides correspondence between instances of the object in and near the object(s); 2) it captures the object interior and is, thus, very suitable for deformation; and 3) it provides the basis for an intuitive object-based multiscale sequence leading to efficiency of segmentation algorithms and trainability of statistical characterizations with limited training sets. As a result of these properties, medial representation is particularly suitable for the following image analysis tasks; how each operates will be described and will be illustrated by results:

1) *segmentation of objects and object complexes via deformable models;*
2) *segmentation of tubular trees, e.g., of blood vessels, by following height ridges of measures of fit of medial atoms to target images;*
3) *object-based image registration via medial loci of such blood vessel trees;*
4) *statistical characterization of shape differences between control and pathological classes of structures.*

These analysis tasks are made possible by a new form of medial representation called m-reps, which is described.

Keywords*—*Discrimination, medial, medical image, multiscale, object, registration, segmentation, shape, statistics.

Manuscript received July 15, 2002; revised March 17, 2003. This work was supported in part by the National Cancer Institute under Grant P01 CA47982, by The Whitaker Foundation under Grant RG-01-0341, by The Foundation of Hope, by Microsoft under an equipment grant, by the Intel Corporation under an equipment grant, and by the University of North Carolina Mental Health and Neuroscience Clinical Research Center under Grant MH33127.

S. M. Pizer is with the Medical Image Display and Analysis Group, Computer Science Department, University of North Carolina, Chapel Hill, NC 27599-3175 USA (e-mail: pizer@cs.unc.edu).

G. Gerig is with the Computer Science Department and Psychiatry Department, University of North Carolina, Chapel Hill, NC 27599-3175 USA (e-mail: gerig@cs.unc.edu).

S. Joshi is with the Medical Image Display and Analysis Group, Radiation Oncology Department, University of North Carolina, Chapel Hill, NC USA (e-mail: sarang@radonc.unc.edu).

S. R. Aylward is with the Medical Image Display and Analysis Group, Radiology Research Laboratory, Radiology Department, University of North Carolina, Chapel Hill, NC 27599-7515 USA (e-mail: aylward@unc.edu).

Digital Object Identifier 10.1109/JPROC.2003.817876

I. Medial Representations

In this paper, we are concerned with object representations for use in three-dimensional (3-D) image analysis methods such as segmentation, registration, and statistical characterization of geometric differences between classes. To support these uses with regard to a population of "object(s)," i.e., single objects, such as kidneys or blood-vessel trees, or object ensembles, such as a liver or kidney pair, it is necessary that each member of the population be effectively captured by the form of representation. For the image analysis objectives described in this paper, we desire that the resulting models be useful for the following:

- statistical characterization of the geometry of a class of object(s) [18] (see Section V);
- segmentation by deforming a model into image intensity data (see Section III-A);
- segmentation by measuring the fit of the local primitive from which the representation is formed to image data either so that
  - ridges of this measure can be used to define the object (cf. Canny edges) (see Section III-B);
  - local statistics of this measure can be used to locate an object section and find its geometric type (slab, tube, sphere) (see [26]).

A variety of object representations have been suggested for 3-D object representation, including landmark sets (e.g., [12]), boundary point distribution models (e.g., [9]), boundary basis function models (e.g., [25]), and atlas-based

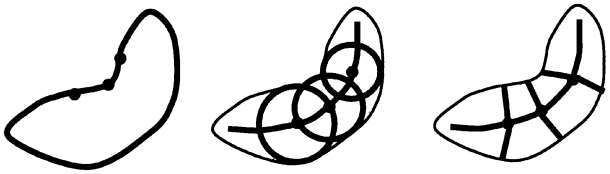

Fig. 1. 2-D figure shown in terms of its boundary, then in terms of bitangent circles wholly interior to the figure, and finally, in terms of medial atoms (see also Fig. 5 for the 3-D case). Individual positions, circles, and medial atoms are shown at sample positions, but in each case, the locus is continuous. The part of this figure that forms the representation is shown in each case with bolder lines.

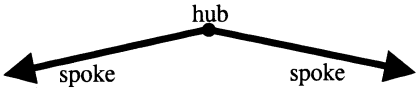

Fig. 2. Medial atom.

voxel displacement models (e.g., [8]). 3-D medial models particularly fit the bill because of a variety of properties that they have, most especially the following.

1) Their inherent geometry provides an object-intrinsic coordinate system and, thus, provides positional and orientational correspondence between instances of the object in and near the object(s).
2) They directly capture the object interior in a compact way and are, thus, computationally suitable for volumetric deformation.
3) They provide the basis for an intuitive object-based multiscale sequence leading to efficiency of segmentation algorithms and trainability of statistical characterizations with limited training sets. In this sequence, objects in an ensemble are described in relation to each other, protrusions and indentations in an object are described in relation to the figure from or into which they extend, and positions interior to and on the boundary of a figure are described in relation to the figure's geometry.

Medial representations of an object have traditionally been seen in terms of the locus of centers and widths of spheres (or in two-dimensional (2-D) circles) that are bitangent to the boundary of the object (Fig. 1), and frequently they have been seen in terms of the centers and widths of bitangent spheres wholly within the object [6]. We have found that a more useful, though mathematically equivalent way of seeing the medial representation is as a locus of "medial atoms," entities made of a hub and two equal length spokes (Fig. 2). The hub is a point at the center of the related bitangent sphere, and the spokes are radii from the center to the points of bitangency. With this view, with an unbranching medial locus for which the locus of hubs forms a smooth surface, the two line segments making up the medial atoms of an unbranching medial locus sweep out the interior of a spatial region that we call a "figure" (Fig. 1). Any point in the interior can be reached by choosing the correct medial atom and traveling an appropriate fraction of the radius out from the hub along one of the spokes. This easy computation is in contradistinction to the difficult computation of the set of interior points from a representation giving just the object boundary.

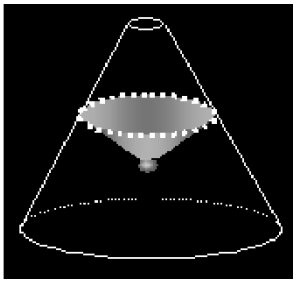

Fig. 3. Section of tube (fine lines) with the cone of medial atoms from a common hub (shown by sphere) intersecting the tube boundary in a circle (dashed bold).

A special, albeit nongeneric case for medial representation are the tubular objects (or object sections)—those with circular cross sections. In these possibly branching tubes, each bitangent sphere is actually tangent to the tube boundary everywhere in a circle (Fig. 3). The medial atoms corresponding to such a bitangent circle share a common hub and a common bisector of their spokes, and these medial atoms are rotations of each other about their common spoke bisector. The locus of the hubs is a space curve in this case, and the common spoke bisector is tangent to this curve. Thus, we can capture a tubular medial locus by a possibly branching curvilinear locus of our ordinary two-spoked medial atoms, with the convention that, for the tubular case, all rotations about the curve's tangent produce additional valid medial atoms.

Blum [6] limited the medial locus to bitangent spheres that were entirely interior to the boundary, and essentially all of the image analysis work with the medial representation has used this form of medial representation. However, with our representations, called *m-reps*, we insist only that the medial atoms themselves be interior to the figure (thus, in the case of and indentation figure, the atom will be exterior to the object). Blum's representation produces a unique equivalent description to an object's boundary, but it produces a branching structure that is typically extremely bushy and complex due to its sensitivity to small-scale boundary pimpling or dimpling, and its branching structure deterministically varies as the particular object instance varies across the population of possible versions of that object or across measurements of these objects from an image. There are some interesting methods for extracting medial models from boundaries (e.g., [24] and [30]) that avoid the bushiness using notions of spatial scale, but even those produce many different branching structures across the population of possible versions of that object or across measurements of these objects from an image. This property, together with the difficulty of deciding at a branch which is the continuation of the limb and which branch, makes it hard to divide such a derived medial locus into figures and subfigures, despite the fact that such subdivision is an important capability of handling objects medially.

The great variability of a medial branching structure across the population makes all of the traditional medial representations useless for the recognition or description of similarly appearing objects. That property also makes the representa-

tion inappropriate for deformable model segmentation since the branching topology would have to change as the object deforms. Nevertheless, the mathematics of the relation between an object boundary and its equivalent Blum medial axis, produced most completely by Giblin and Kimia [17], is useful in dealing with the new medial representation that we have developed, i.e., m-reps.

In contrast to the Blum case, in an m-rep, the medial branching structure of an object into figures and attached subfigures is fixed for the whole population by a training stage. This structure is then fit either to an object given by a boundary or to an image. Such medial determination by fitting a medial model with a fixed branching structure is a stable process in contrast to the unstable process of inferring a medial structure from a single boundary. Smooth boundaries are inferred from the medial structure and then displaced along their normals by a boundary displacement component of the m-rep to handle the small-scale pimples or dimples or, in the case of tubes, the small-scale deviations from circularity of the tubular cross sections. The fixed branching structure allows a medial representation to achieve its long noted potential in regard to the aforementioned applications of segmentation and of statistical characterization of the geometry of a class of object(s).

The mathematics of this synthesis of a boundary from a medial representation has been developed by Damon [11]. In this mathematics, the conditions for a given m-rep producing a smooth unfolded boundary and the relation between the differential geometry of the m-rep and the differential geometry of the boundary are given.

The medial structure is determined by analyzing a population of training objects starting from their boundaries [29]. This process is stabilized by the use of the population, or the medial structure is known from anatomy; e.g., most blood-vessel trees can be assumed to be trees of tubes with binary branching.

Deformation of an m-rep with a fixed branching structure allows stable segmentation and stable comparison of objects in a population of a given name, e.g., the brain structures called hippocampi. M-reps also allow a consistent description of object ensembles, describing not only the individual objects in an ensemble, but also the geometric relationships between objects. In addition, m-reps allow access to image data in coordinates that we call "object-intrinsic" because they yield correspondences in spatial position and in spatial directions across different instances of an object and its associated image. It is thus easily possible to make image templates in these object-intrinsic coordinates that allow comparison with a particular target image relative to a candidate object's geometry.

Fig. 4 shows the basic primitive of medial representation of the 3-D object(s), the *medial atom*, formed from a medial hub point (visualized as a ball) from which issue two spoke vectors of equal length (visualized as arrows). The atom implies that a boundary approximately passes through and is orthogonal to the ends. The atom carries its own coordinate system, with the medial point forming the origin; the bisector $\vec{b}$ of the spokes, the orthogonal complement vector $\vec{n}$

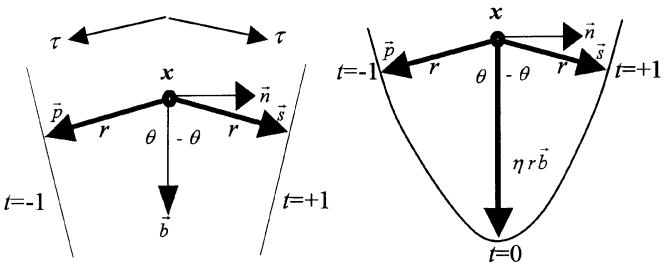

Fig. 4. Medial atom (in bold), its coordinates, and its implied boundary sections. (*left*) An atom internal to the medial locus. (*right*) An atom at endpoints of the medial locus.

in the plane of the spokes, and their orthogonal complement forming the coordinate frame, and the common spoke length r forming the unit of distance.

Image analysis of objects requires measuring the fit of the object model or its primitives to the expected behavior of image intensities near the object boundary or in and near the interior of the object. This can be accomplished through the measurement of the fit of a medial atom $\underline{m}$ based on the behavior of the image function in the medial coordinates. For example, one can measure the degree to which the image has contrast of the appropriate polarity at and orthogonal to both spoke ends. We call this scalar measurement of image match $\mathrm{M}(\underline{m})$, the *medialness* of $\underline{m}$ in the image.

Simple medial loci in 3-D represent solid elements called figures. Figures are formed as 2-D sheets or space curves of medial atoms. It can be shown that the vector $\vec{n}$ must be orthogonal to this locus. Also, if the locus is a curve, the atom must imply a circle of spokes formed by rotating the spokes about the $\vec{b}$ vector, with the boundary implied at each spoke in the circle, and the associated medialness must integrate the image match over all of these spokes.

Models are formed as sets of branching structures with these simple medial loci as the roots and branches. At the ends and branches of these structures, special properties apply.

The following three forms of medial locus representations have been described.

1) Linked lists of medial atoms that are next to each other to within the resolution of the image data [2], [21] (Fig. 9, left-hand side).
2) Discrete m-reps (*dm-reps*) whose figures are formed as meshes or chains of discrete medial atoms [22] (Fig. 5, top). In dm-reps, end atoms include a third spoke formed in the direction of the bisector between the other two spokes and of length ηr, with $\eta \geq 1$ (Fig. 4) controlling the sharpness of the crest. Attached subfigures in dm-reps ride on the implied boundary of a parent figure.
3) Continuous m-reps (*cm-reps*) whose figures are formed as b-splines of (x, y, z, r) [34] (Fig. 5, bottom). The end curves of these medial manifolds are places that satisfy $|\nabla r| = 1$, where the gradient is taken with respect to Euclidean distance on the medial manifold. At present, these are restricted to single figure objects.

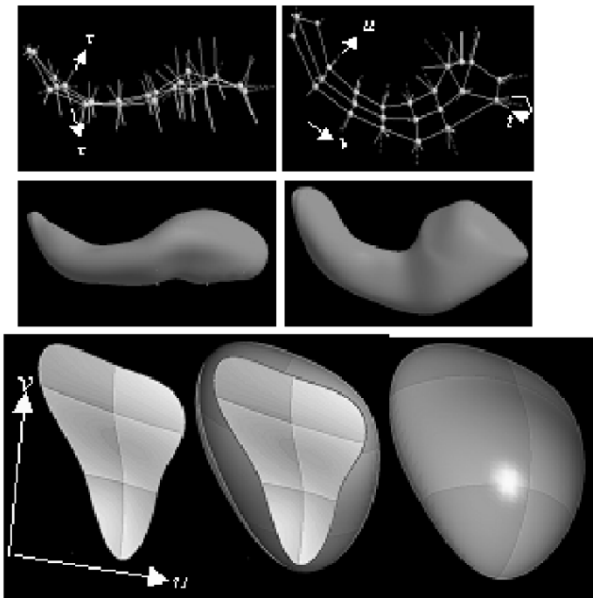

Fig. 5. 3-D medial locus representations. (*top*) dm-rep. (*bottom*) cm-rep.

In all of these, the boundary is easily computable from the medial representation. The means of doing so from discrete m-reps using a modified form of the subdivision surfaces method [7] and constraints against boundary folding [11] has been developed by Thall [31][1].

M-reps provide object-intrinsic coordinates for all of three-space included in a figure and exterior to it out to its focal surface, with these coordinates being suited for shape characterization by being magnification invariant at both global and local levels of scale. For a single figure, these *figural coordinates* are (u, v, t, τ). The coordinates (u, v) (or u alone for tubular figures) characterize position on the medial locus with distances along the locus measured in r-proportional terms. The coordinate $t \in [-1, 1]$ indicates which side of the medial locus the point is; for internal medial points, $t = +1$ or -1, and for medial locus endpoints, t runs continuously around the crest region connecting the two boundary sides, going from -1 to 0 at the crest to $+1$. The coordinate τ measures the distance (in r-proportional terms) along spokes from the implied boundary with $\tau > 0$ outside the implied boundary, $\tau < 0$ inside the implied boundary, and $\tau = -1$ at the medial locus. For multifigure objects, the point's closest figure must also be indicated and, for dm-reps, a blend region between the subfigure and its host figure must be computed with a coordinate w taking one along the blend (Fig. 6, left-hand side). For object ensembles [13], the geometric relationship of neighboring objects are recorded: parts of the medially implied boundary of one object that are near the neighbor are known not only in its own figural coordinates, but also its neighbor's figural coordinates (Fig. 6, right-hand side).

In populations or deformations of object(s) represented by a single branching topology, positional (and orientational and

[1][Online]. Available: http://midag.cs.unc.edu/pubs/papers/Thall_TR02-001.pdf

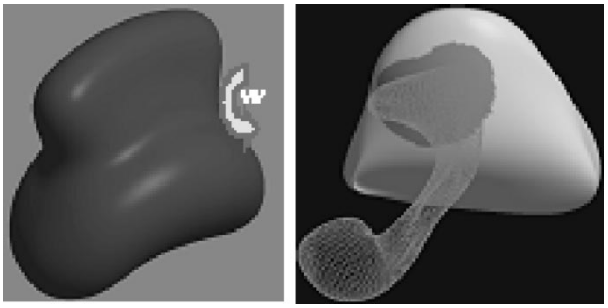

Fig. 6. Figural coordinates: (*left*) for blend regions of multifigure objects and (*right*) for object ensembles: darker region of bladder shows locations τ bone $<$ a threshold.

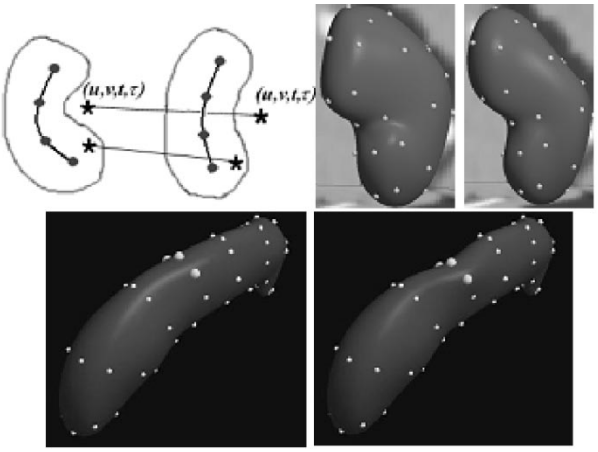

Fig. 7. Positionally corresponding points via figural coordinates. (*top left*) Points in two-space. (*top right*) Boundary points in a deforming kidney. (*bottom*) Boundary points in a statistical principal component analysis medial atom eigenmode on a hippocampus.

metric) correspondence between instances of the object(s) is defined by having the same figural coordinates (Fig. 7). Image intensities for any element of the population of objects are also represented in an object-intrinsic and, thus, stable way by using figural coordinates.

Medial representations allow representations at many object- and figure-related scale levels. These allow the characterization of geometric changes to have locality. They lead to efficiency via coarse-to-fine algorithms and to stable statistical characterizations with few training samples via Markov random fields. The scale levels that we presently use, together with the geometric transformations allowed at each level and the neighboring entities at each scale level, are given in Table 1. Each transformation is thought of as a residue with respect to the larger scale levels.

II. Medial Representations of Populations of Objects or Object Ensembles

Using the method of Styner, one can take a training sample from a population of objects, each represented as a characteristic image, and produce a common figural topology and dm-rep sampling that can be deformed into any member of the population with a criterion level of accuracy. Let $\underline{\mathbf{z}}^k$ be the geometric representation at scale level k, and let $\underline{z}_i^k$

Table 1
Geometry by Scale Level (Please Read the Two Portions of the Horizontally Adjacent)

Scale level k	Geometric entity	Transformation S^k
1	Object ensemble	Similarity
2	Object	Similarity
3	Figural	Similarity in figural coordinate of its host's figural boundary, plus hinging and elongation
4	Through section of figure (medial atom)	Medial atom change
5	Boundary vertex	Displacement along medially implied normal

Primitive $\underline{z}^k_i$	Neighbors $\underline{N}(\underline{z}^k_i)$	Comments
Object ensemble pose		
Object pose	Adjacent objects	
Figural pose in host's cords & elongation	Adjacent figures, possibly attached to same host	
Medial atom value	2-4 adjacent medial atoms	Repeatable at various levels of medial sampling
Boundary vertex position	Adjacent boundary vertices	Repeatable at various levels of boundary sampling

be the representation of the ith primitive at scale level k. Each primitive $\underline{z}^k_i$ has a small set of neighbors $\underline{N}(\underline{z}^k_i)$ at scale level k (see Table 1) and a parent primitive $P(\underline{z}^k_i)$ at scale level $k-1$, but of the same type as $\underline{z}^k_i$. Also associated with scale level k is a type of transformation S^k such that $\underline{z}^k_i = S^k(P(\underline{z}^k_i))$. Let the parameters $\underline{\delta}^k_i$ of that transformation S^k represent the residue between $\underline{z}^k_i$ at scale level k and $P(\underline{z}^k_i)$ at scale level $k-1$. We do statistics via Markov random fields by estimating the parameters of the probability distributions of $p(\underline{z}^k_i \text{ relative to } P(\underline{z}^k_i), \underline{z}^k_i \text{ relative to } \underline{N}(\underline{z}^k_i))$, where the first term is measured by $\underline{\delta}^k_i$. This can be done, for example, using a form of principal components analysis adpated to Lie groups [14]. The object-intrinsic correspondences given by the medial representation make such analysis possible. Estimating the probabilities class by class (e.g., for a control class and pathological class) allows the study of the differences between the probability distributions at any chosen scale level.

At any scale level, this representation and Markov statistics divide geometric distinctions between classes into the geometric parameters described at that scale level. For example, at the object scale level, distinctions are made in translations, rotations, and uniform scalings. At the medial atom (figural section) scale level, the representation divides shape changes into natural categories of elongation, thickening, bending, and twisting. At the boundary displacement scale level, it allows the characterization of local properties of surface texture.

III. Segmentation via Medial Representations

A. Segmentation via Deformable m-rep Models

Segmentation of images by deforming an m-rep model, detailed by Joshi *et al.* in [20], is based on a Bayesian framework, scale level by scale level, coarse to fine. At each scale level, the model is transformed to produce the model for the next smaller scale. The paradigm at each scale level k is to find, from the transformations appropriate to that scale level (see Table 1), that transformation S^k of template $P(\underline{z}^k_i)$, producing $\underline{z}^k_i$, such as to maximize the posterior $p(\underline{z}^k_i|\text{data})$ or equivalently to maximize $\log p(S^k \text{ at } P(\underline{z}^k_i)) + \log p(\text{data}|\underline{z}^k_i)$, where $p(S^k \text{ at } P(\underline{z}^k_i))$ is the prior probability density capturing the geometric typicality of the anatomic object residue S^k at $P(\underline{z}^k_i)$, and $p(\text{data}|\underline{z}^k_i)$ is the data likelihood function capturing the image data-to-geometry relationship. At each stage, we divide $\log p(S^k \text{ at } P(\underline{z}^k_i))$ into the sum of a parent term and a neighbor term. The parent term is $\log p(\underline{\delta}^k_i)$, i.e., the log probability density of the residue of $\underline{z}^k_i$ relative to the parent $P(\underline{z}^k_i)$. The neighbor term is $\log p(\underline{z}^k_i \text{ relative to its neighbors } \underline{N}(\underline{z}^k_i))$. At the medial atom scale level, the relation to the neighbors guarantees the smoothness of the medial manifold. Each level's result provides both an initial value and a prior for the primitives at the next smaller scale level. The transformation at the smallest scale level is a dense displacement field applied to the boundary of the figure on the scale of the voxel resolution of the imaging modality. As the vector field is not medially based, the small-scale boundary features are robustly accommodated.

We have begun estimating these probabilities from training sets of objects. However, at present, the prior is induced on the above transformation based on the displacement of the implied boundary of the objects. Throughout, an independent Gaussian prior on boundary displacement is used with variance proportional to the local radius. Good association between points on the original object boundary and the deformed boundary is made using the figural coordinate system describe in the above section. At the boundary vertex scale level, the prior is induced on the dense displacement field using a Markov random field prior derived from energetics associated with thin elastic membranes to guarantee smoothness.

Having defined the geometric typicality (prior) energetics, we now define the data likelihood function measuring geometry to image match. In the future, we will compute this function using multiscale probabilities, but at the present, we compute it as the correlation between a predefined rms-normalized zero-mean template image I_{template} and the rms-normalized version of the target image I_{data} in the neighborhood of the boundary B implied by $\underline{\mathbf{z}}^k$. The neighborhood is defined by $|\tau| < \tau_{\max}$, a collar around B, and the integration in the correlation is along τ and B. This association between points in the template image and the data image is made using the object intrinsic coordinate system described above.

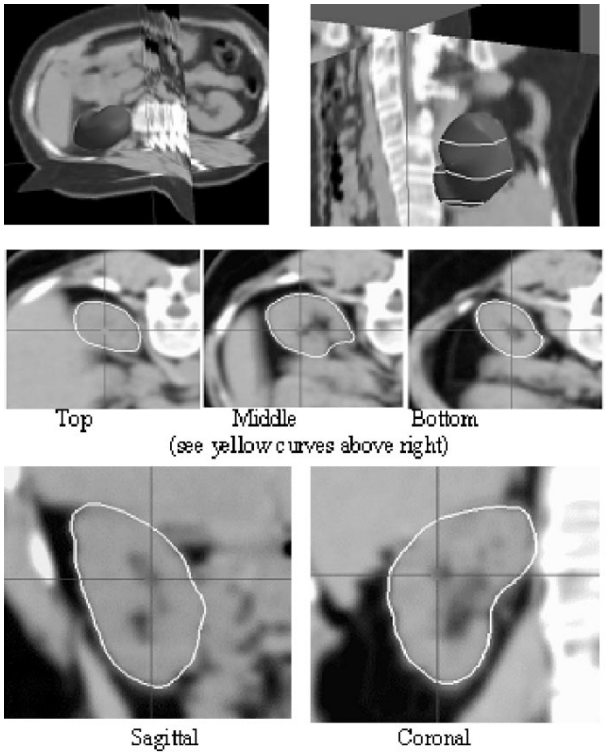

Fig. 8. Result of kidney segmentation from CT by deformable m-reps. The accuracy in this case is the median among the 24 kidneys extracted.

We have been using two basic types of templates: an analytical template computed from derivatives of the Gaussian and an empirical template learned from an example image from which the template medial model was built. Using the data likelihood defined above and the prior defined in the above section, the log posterior is defined as a weighted sum of the two terms, with weights chosen by the user. For optimizing the posterior with respect to the similarity transformations at scale levels 1–3 and the local atom-by-atom transformation at scale level 4, we use a conjugate gradient optimization algorithm; for optimizing the posterior with respect to the dense displacement field at the boundary vertex scale level, we use a simple steepest decent algorithm.

To run the segmentation, the user takes a few seconds to rigidly place the template model in the target data set. This initialization of the algorithm is followed by the automatic hierarchical segmentation, which, in the present implementation, takes under 5 min for convergence. This speed, for the accuracy of segmentation produced, is a direct result of the multiscale form of the object representation and, thus, of the deformable model algorithm.

We have used this segmentation procedure for extracting a variety of 3-D anatomic objects, of which one is the kidney parenchyma plus the renal pelvis, in subjects undergoing radiation treatment for cancer. In [23], we present results on 24 kidney extractions from computed tomography (CT) showing segmentation that succeeds in every case and has an agreement with human segmentations comparable to that of humans with each other (see Fig. 8 for an example).

B. Segmentation via Medial Representations of Tubular Geometry

Tubular objects are multidimensional generalized cylinders; their paths may be tortuous, may branch, and may contain cycles; and their radii will vary smoothly along those paths. In 3-D, magnetic resonance angiogram (MRA) and X-ray CT images much of human anatomy appears tubular, e.g., blood vessels, bronchi, bowel, nerves, and selected bones.

In Section I, we indicated that tubes in 3-D can be represented by a space curve of medial atoms, whose centers form the central axis of the tube and whose spokes are rotated about their bisector to generate the circularly symmetric cross section that we take to be the definition of a tube. The symmetry inherent in medial representations enables simple and fast methods for generating tubular segmentations using this representation from 3-D images and for registering images according to those tubular structures. The general approach is to find a locus of medial atoms that form a maximum convexity ridge of medialness of the image, i.e., a 2-D maximum, orthogonal to the ridge, of the medial fit to the image data.

We and others [1], [2], [4], [15] have developed such methods for forming medial segmentations of tubular objects that take particular advantage of the scale-space and symmetry properties of images of tubes. In particular, for a wide range of scales, a tubular object in an image will have stable one-dimensional (1-D) central maximum convexity ridge of the medialness function formed simply as image intensity. By first solving for the central intensity ridge to represent a central axis and then using that central axis to stabilize a radius estimation process based on boundary strength integrated around the circle of medial spokes, medial representations of tubes can be quickly formed. By incorporating optimal scale and zoom invariant measures during traversal and radius estimation, the representation generation process remains insensitive to intensity and boundary noise. For example, given MRA volume data of intra-cranial vasculature, the system can form representations of that vasculature with sub-voxel accuracy, i.e., an average error was less than 0.5 voxel and consistency was sub-voxel such that greater than 80% of the central axis points were within one voxel. The primary benefit of decoupling the central-axis and radius estimation processes is that the time to generate a representation is sped by the isolation of their parameter spaces during optimization. For example, extraction of over 400 vessel segments in a typical intra-cranial MRA volume image requires approximately 15 min [1].

Our centerline extraction method operates by an iterative dynamic-scale step-maximize procedure. The eigenvectors of the local scaled Hessian of the image intensity medialness function at one ridge point are used to approximate the tangent and normal directions of the ridge (Fig. 9, left-hand side). That normal plane is shifted in the tangent direction to bound the search for a connecting ridge point at which the next medial atom in the chain is centered. The local 2-D

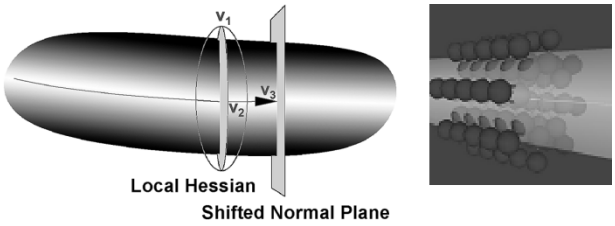

Fig. 9. (*left*) Eigenvectors $(\mathbf{v}_1, \mathbf{v}_2, \mathbf{v}_3)$ of the local Hessian approximate the tangent $(\mathbf{v}_3)$ and normal $(\mathbf{v}_1, \mathbf{v}_2)$ directions of the ridge. Shifting the normal plane in the tangent direction bounds the search for the next ridge point. (*right*) Series of binary medialness kernels centered on and normal to the ridge are applied at different scales to determine the local radius of the tube.

maximum intensity point in that plane is a ridge point if its normal direction eigenvalues are negative. We also verify that its cross-sectional intensities are circularly symmetric by validating that the eigenvalues in the normal directions are nearly equal. When singularities are encountered, we detect the swapping of the eigenvectors of the Hessian, and since singularities are nongeneric, slightly changing the scale being used to traverse the ridge causes those singularities to move or be destroyed and traversal along one branch continues. Our dynamic-scale traversal method passed across branchpoints ~90% of the time, depending on the level of noise in the image. Furthermore, the method's performance was not statistically significantly dependent on its parameters or initial conditions.

The local radius of the tube determines the scale of the measures used during ridge traversal. The local radius of a tube is determined by an additional 1-D maximum convexity ridge operation (i.e., extremum) of medialness in the medial atom's r dimension, as applied to a medialness function on medial atoms centered on the previously extracted axis curve, but with a variable radius and object angle. The method evaluates multiple medialness kernels on neighboring ridge points (Fig. 9, right-hand side), orienting those kernels' frames parallel and orthogonal to their axis curves, and it thereby determines the radius of those kernels that produces a maximal medialness response.

IV. Registration via Medial Representations of Tubular Objects

The medial geometry of tubular objects can also be exploited to speed the registration of a tubular representation to an image. The registration metric measures how well the central axes in a representation map to the ridges in a target image. The orientation and scale of the representations are used to constrain a coarse-to-fine registration optimization process such that a vessel curve segment whose medial tangent vector is $\vec{b}$ is only used to resolve alignment orthogonal to $\vec{b}$. The sparseness of the representations also speeds the registration process. Representations formed using data from one modality can be registered with data from different modalities. Monte Carlo experiments demonstrate subvoxel accuracy, subvoxel consistency, and registration times on the order of seconds [3]. In Fig. 10, the vessel representations from one CT scan of a patient are aligned with another scan

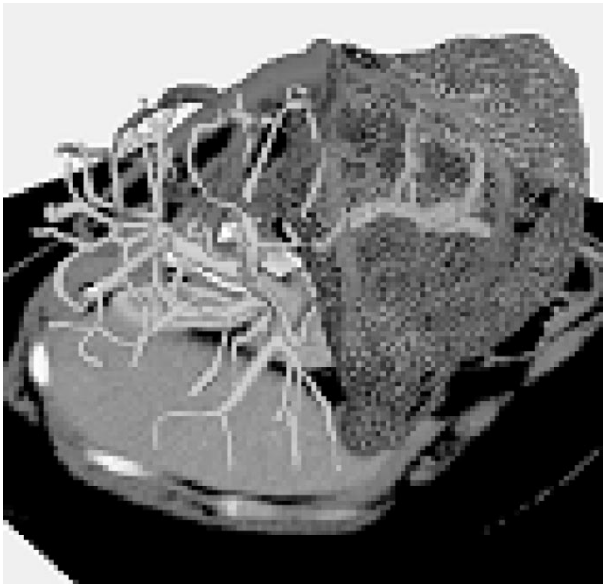

Fig. 10. Blood vessels from two liver CT scans have been registered to capture blood inflow and outflow. The vessels are shown with the right lobe of the liver to facilitate partial liver transplant planning.

that captures a different vascular system. Viewing vessel representations from both scans facilitates liver transplant planning. These methods are also being used to register preoperative vascular representations with intra-operative images, such as 3-D ultrasound images, so that preoperative plans can be overlaid onto the intra-operative data for surgical guidance.

V. Statistical Shape Characterization via Medial Representations

Besides providing shape models for segmentation by deformable models, the parametrizations of geometric objects provided by the various representations can also serve as a data structure for statistical shape analysis. Medial representations have particular strengths because their intrinsic coordinates produce positional correspondences that lead to sensitivity to small differences between classes of objects and because the way they support multiscale representation and the related probabilistic representation by Markov random fields allows training of the probabilities that is efficient in the number of training samples required. Indeed, there are a very large number of probability density functions that must be trained (both a parent-relative and a neighbor-relative density for each primitive $\underline{z}_i^k$ at each scale level), but each can be trained from the same training sample, and the small number of parameters of each probability density leads to few training samples being required.

Neuroimaging is a research area where geometric analysis can provide information about changes of brain structures due to disease. Structural imaging studies thus far have most often focused on volumetric assessment of brain structures, e.g., full brain or hemispheric gray and white matter, ventricular volume, and hippocampus. Increasing evidence for structural changes in small subregions and parts of structures

drive development of new structure analysis techniques. In [33], Wang *et al.* found that, while hippocampal volume did not discriminate schizophrenia groups from control groups, shape measurements did provide a distinct group separation. This paper further discusses that summary comparisons of whole structures, as used in conventional volumetric analysis, ignores the possibility of detecting regional differences. Csernansky *et al.* [10] suggests that a full characterization of neuroanatomical abnormalities will increase our understanding of etiology, pathogenesis, and pathophysiology of schizophrenia. Results show that the analysis of hippocampal shape discriminates schizophrenia and control subjects with greater power than volumetry [19]. All these studies and many studies by Toga and Thompson [32] advocate new morphometry techniques to study shape rather than gross volume and to provide quantitative measures that are not only statistical significant, but also neuroanatomically relevant and intuitive.

As discussed above, compared to other geometric parameterizations, m-reps provide advantages of locality and sensitivity (when used as multiscale residues), intuitiveness of results, and robustness against limited training samples. In our research to date, we have found that when used globally, m-reps give similar results to other representations such as point distribution models, voxel displacement models, and spherical harmonic models. We illustrate the method with the following clinical study of the shape of the lateral ventricles in schizophrenia using dm-reps.

Lateral ventricle findings are often reported in neuroimaging studies. Ventricles are fluid space that are altered in diseases causing brain atrophy, e.g., Alzheimer's disease, or whose volume is affected by neuropathology, e.g., schizophrenia. We describe a study that serves an example for many other ongoing morphometric brain studies. A twin study includes healthy identical twins [monozygotic (MZ)], nonidentical twins [dizygotic (DZ)], identical twins discordant for schizophrenia (MZ–DS) (one co-twin schizophrenic, other co-twin subject at risk), and nonrelated (NR) subjects. This study allows us to test several hypotheses related to genetics and disease, e.g., similarity of ventricle shape among co-twins with varying genetic similarity, or shape alteration of ventricles due to disease in the MZ–DS group. The ventricle shapes were segmented from 3-D magnetic resonance images using automatic tissue classification and manually guided postprocessing. The surfaces of the left and right ventricles have been parametrized using spherical harmonics [16], [27], [28], spatially aligned using Procrustes fit of homologous surface points (PDM model [9]), and transformed into medial m-rep representations [27]–[29]. In this study, for each medial atom in the fixed topology m-rep, the population of that particular atom is statistically studied. The multiresolution residue approach discussed earlier will be applied in future research.

Fig. 11 illustrates right and left ventricle pairs of co-twins with an m-rep mesh and implied surface. The local radii are overlaid as balls with varying size and color. Local width differences between co-twins can be tested by comparing the width attributes at mesh points that are homologous according to figural coordinates. Fig. 11 illustrates co-twin differences of right, but not left ventricles, well localized in the atrium part of the ventricles. Fig. 12 shows the result of a statistical analysis of MZ versus DZ versus NR pairs. The results demonstrate the better shape similarity of ventricles of identical MZ twins as compared to DZ twins and NR subjects.

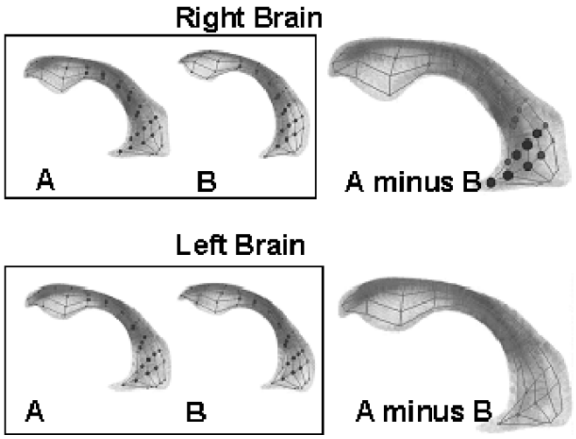

Fig. 11. Shape comparison of ventricles based on medial representations. The larger figures represent the medial mesh with width (radius) difference at corresponding mesh points. The size of the disks indicate local differences between twins A and B in the range of -0.3–1.5 mm.

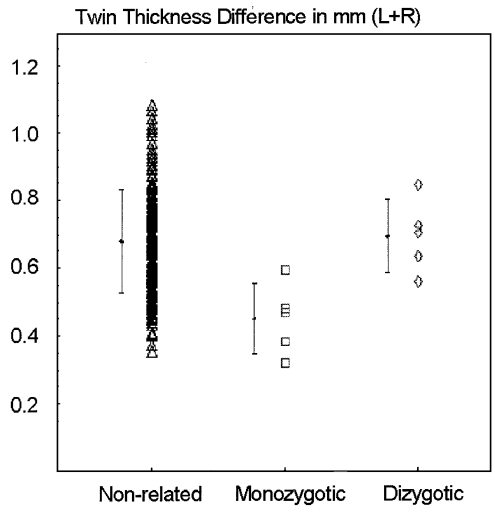

Fig. 12. Statistics of ventricle similarities. The mean absolute width differences at corresponding mesh points between co-twins is shown for the three groups nonrelated pairs (180 pairs, left), MZ twins (five pairs, middle) and DZ twins (five pairs, right). The plot demonstrates that the DZ twin results could be a subset of the population of unrelated pairs (nonsignificant group difference $p < 0.8562$) with smaller variance due to the larger age/gender/sibling similarity. The MZ twins, however, are significantly different from the DZ ($p < 0.0065$) and from the unrelated subjects ($p < 0.0009$).

Similar to the width attributes describing local growth, we also analyzed figural bending by comparing the mesh atom positions relative to a template and by measuring local mesh curvature. In ongoing studies, we extend the single figure analysis of lateral ventricles to multifigure analysis of the whole ventricular system and, finally, to a multiob-

ject analysis including ventricles in the context of abutting structures (hippocampus, caudate nucleus, putamen, pallide globe). Moreover, our studies of the hippocampus are being extended [35] to leverage the properties of cm-reps that they analytically parameterize a medial locus and, thus, provide a basis for improvement of the homology across members of the population of objects (here, hippocampi) via the registration (diffeomorphism of the medial locus) of geometric measurements at a variety of scale levels.

VI. Conclusion

We have described the framework of stable medial representation and its theoretical advantages for image analysis. By describing its use for a variety of segmentation, registration, and statistical shape characterization objectives, we have illustrated the usefulness of this framework. Our work in these areas continues. In particular, there are many steps left in the full development of the statistical framework based on Markov residues and its use for both segmentation and shape characterization. Also, methods and programs for the use of multifigure and multiobject models [13] are well along, but require further work. Additional validations are on our agenda. Also, mechanical methods on m-rep models to estimate and analyze intrapatient deformations are being developed.

Acknowledgment

The authors are grateful to conceptual, geometric, algorithmic, or code contributions from P. T. Fletcher, P. Yushkevich, C. Lu, M. Styner, E. Bullitt, A. Thall, and S. Ho. The authors thank E. Chaney, G. Tracton, and J. Lieberman for providing images and driving problems for segmentation or statistical shape characterization. The authors also thank D. Bull for help with the preparation of this paper's manuscript.

References

[1] S. Aylward, E. Bullitt, S. M. Pizer, and D. Eberly, "Intensity ridge and widths for tubular object segmentation and registration," in *IEEE Mathematical Methods in Biomedical Image Analysis Workshop*, 1996, pp. 131–138.

[2] S. Aylward and E. Bullitt, "Initialization, noise, singularities, and scale in height ridge traversal object centerline extraction," *IEEE Trans. Med. Imaging*, vol. 21, pp. 61–75, Feb. 2002.

[3] S. Aylward, J. Jomier, J. P. Guyon, and S. Weeks. Intra-operative 3D ultrasound augmentation. presented at Proc. IEEE Int. Biomedical Imaging Symp. 2002. [CD-ROM]

[4] E. Bullitt, S. Aylward, K. Smith, S. Mukherji, M. Jiroutek, and K. Muller, "Symbolic description of intracerebral vessels segmented from magnetic resonance angiograms and evaluation by comparison with X-ray angiograms," *Med. Image Analysis*, vol. 5, pp. 157–169, 2001.

[5] A. J. Bartley, W. J. Douglas, and D. R. Weinberger, "Genetic variability of human brain size and cortical gyral patterns," *Brain*, vol. 120, pp. 257–269, 1997.

[6] H. Blum, "A transformation for extracting new descriptors of shape," in *Models for the Perception of Speech and Visual Form*, W. Wathen-Dunn, Ed. Cambridge, MA: MIT Press, 1967, pp. 363–380.

[7] E. Catmull and J. Clark, "Recursively generated B-spline surfaces on arbitrary topological meshes," *Computer-Aided Design*, vol. 10, pp. 183–188, 1978.

[8] G. E. Christensen, S. C. Joshi, and M. I. Miller, "Volumetric transformation of brain anatomy," *IEEE Trans. Med. Imaging*, vol. 16, pp. 864–877, June 1997.

[9] T. F. Cootes *et al.*, "Active shape models—Their training and application," *Comput. Vis. Image Understanding*, vol. 61, no. 1, pp. 31–59, 1995.

[10] J. Csernansky, S. Joshi, L. Wang, J. Haller, M. Gado, J. Miller, U. Grenander, and M. Miller, "Hippocampal morphometry in schizophrenia via high dimensional brain mapping," in *Proc. Nat. Academy of Science*, vol. 95, 1998, pp. 11 406–11 411.

[11] J. Damon. (2002) Determining the geometry of boundaries of objects from medial data. Dept. Math., Univ. North Carolina, Chapel Hill, NC. [Online]. Available: http://midag.cs.unc.edu/pubs/papers/DamonJ02.pdf

[12] I. Dryden and K. V. Mardia, *Statistical Shape Analysis*. Chichester, U.K.: Wiley, 1998.

[13] P. T. Fletcher, S. M. Pizer, G. Gash, and S. Joshi. Deformable m-rep segmentation of object complexes. presented at IEEE Int. Biomedical Imaging (ISBI) Symp. 2002. [CD-ROM]

[14] P. T. Fletcher, C. Lu, and S. Joshi, "Statistics of shape via principal geodesic analysis on lie groups," in *Proc. IEEE CVPR*, vol. I, 2003, pp. 95–101.

[15] A. F. Frangi, W. J. Niessen, R. M. Hoogeveen, T. van Walsum, and M. A. Viergever, "Model-based quantitation of 3-D magnetic resonance angiographic images," *IEEE Trans. Med. Imaging*, vol. 18, pp. 946–956, Oct. 1999.

[16] G. Gerig, M. Styner, M. E. Shenton, and J. A. Lieberman, "Shape versus size: Improved understanding of the morphology of brain structures," in *Proceedings of MICCAI*. New York: Springer-Verlag LNCS, 2001, vol. 2208, pp. 24–32.

[17] P. Giblin and B. Kimia, "A formal classification of 3D medial axis points and their local geometry," in *Proc. IEEE CVPR*, vol. 11, 2000, pp. 566–573.

[18] U. Grenander and M. I. Miller, "Computational anatomy: An emerging discipline," *Q. Appl. Math.*, vol. 56, pp. 617–694, 1998.

[19] J. Haller, A. Banerjee, G. E. Christensen, S. C. Joshi, M. I. Miller, M. W. Vannier, and G. Csernansky, "Three-Dimensional hipocampal volumetry by high dimensional transformation of a neuroanatomical atlas," *Radiology*, vol. 202, pp. 504–510, 1997.

[20] S. Joshi, S. Pizer, P. T. Fletcher, P. Yushkevich, A. Thall, and J. S. Marron, "Multiscale deformable model segmentation and statistical shape analysis using medial descriptions," *IEEE Trans. Med. Imaging*, vol. 21, pp. 538–550, May 2002.

[21] S. Pizer, D. Eberly, B. S. Morse, and D. Fritsch, "Zoom-invariant vision of figural shape: The mathematics of cores," *Comput. Vis. and Image Understanding*, vol. 69, pp. 55–71, 1995.

[22] S. Pizer, D. Fritsch, V. Johnson, and E. Chaney, "Segmentation, registration, and measurement of shape variation via image object shape," *IEEE Trans. Med. Imaging*, vol. 18, pp. 851–865, Oct. 1996.

[23] S. Pizer, P. T. Fletcher, S. Joshi, A. Thall, Z. Chen, Y. Fridman, D. Fritsch, G. Gash, J. Glotzer, M. Jiroutek, C. Lu, K. Muller, G. Tracton, P. Yushkevich, and E. Chaney, "Deformable m-reps for 3D medical image segmentation," *Int. J. Comp. Vision*, vol. 55, no. 2, pp. 85–106, Nov./Dec. 2003.

[24] K. Siddiqi, S. Bouix, A. Tannenbaum, and S. Zucker, "Hamilton–Jacobi skeletons," *Int. J. Comput. Vision*, vol. 48, pp. 215–231, 2002.

[25] L. H. Staib and J. S. Duncan, "Model-based deformable surface finding for medical images," *IEEE Trans. Med. Imaging*, vol. 15, pp. 1–12, May 1996.

[26] G. Stetten and S. M. Pizer, "Medial node models to identify and measure objects in real-time 3D echocardiography," *IEEE Trans. Med. Imaging*, vol. 18, pp. 1025–1034, Oct. 1999.

[27] M. Styner and G. Gerig, "Medial models incorporating object variability for 3D shape analysis," in *Proceedings of IPMI*. New York: Springer-Verlag LNCS, 2001, vol. 2082, pp. 502–516.

[28] ——, "Three-dimensional medial shape representation incorporating object variability," in *Proc. IEEE Computer Vision and Pattern Recognition*, 2001, pp. 651–656.

[29] M. Styner, G. Gerig, S. Joshi, and S. Pizer, "Automatic and robust computation of 3D medial models incorporating object variability," *Int. J. Comput. Vision*, vol. 55, no. 2, pp. 107–122, Nov. 2003.

[30] G. Székely, "Shape characterization by local symmetries," in *Habilitation*. Zurich, Switzerland: Swiss Fed. Inst. Technol., 1996.

[31] A. Thall, "Fast C^2 interpolating subdivision surfaces using iterative inversion of stationary subdivision rules," Comput. Sci. Dept., Univ. North Carolina, Chapel Hill, NC, [Online]. Available: http://midag.cs.unc.edu/pubs/papers/Thall_TR02–001.pdf, 2002.

[32] A. W. Toga and P. M. Thompson, "The role of image registration in brain mapping," *Image Vis. Comput.*, vol. 19, pp. 3–24, 2001.
[33] L. Wang, S. C. Joshi, M. I. Miller, U. Grenander, and J. G. Csernansky, "Statistical analysis of hippocampal asymmetry," *NeuroImage*, vol. 14, pp. 531–545, 2001.
[34] P. Yushkevich, P. T. Fletcher, S. Joshi, A. Thall, and S. Pizer, "Continuous medial representations for geometric object modeling in 2D and 3D," *Image Vis. Comput. (Special Issue on Generative Model-Based Vision)*, vol. 21, no. 1, pp. 17–27, 2003.
[35] P. Yushkevich, S. M. Pizer, S. Joshi, and J. S. Marron. (2002) Improving the locality of statistical shape analysis in the context of medial representation [Online]. Available: http://midag.cs.unc.edu/pubs/papers/IJCV01-Yushkevich.pdf

Stephen M. Pizer (Senior Member, IEEE) received the Bachelor degree in applied mathematics from Brown University, Providence, RI, in 1963, and the Ph.D. degree in computer science from Harvard University, Cambridge, MA, in 1967.

He is currently the Kenan Professor of Computer Science, Radiology, Radiation Oncology and Biomedical Engineering at the University of North Carolina (UNC), Chapel Hill. He heads UNC's multidepartmental Medical Image Display and Analysis Group, a collaborative group of approximately 100 professionals from the Departments of Computer Science, Radiology, Radiation Oncology, Surgery, Psychiatry, Neurology, Statistics, Mathematics, Biostatistics, and Biomedical Engineering. He also co-leads the Computer Science's Graphics and Image Laboratory. Since 1962, his research has focused on medical image processing and display and covers human vision, multiscale, geometric computer image analysis, interactive 3-D graphics, and contrast enhancement. His recent focus has been on medial models of the geometry of objects and multiobject complexes and the use of these models in 3-D image segmentation and statistical characterization of object geometry. He has active collaborations with laboratories in The Netherlands, Germany, Denmark, Austria, and the U.S.

Dr. Pizer is an Associate Editor for the IEEE TRANSACTIONS ON MEDICAL IMAGING.

Guido Gerig (Member, IEEE) received the Ph.D. degree from the Eidgenössische Technische Hochschule (ETH), Zurich, Switzerland, in 1987.

He is currently the Taylor Grandy Professor with joint appointments with the Computer Science and Psychiatry Departments, University of North Carolina, Chapel Hill. In 1985, he began research in the area of medical image analysis at the ETH. Since then, he has led a large number of national and international projects with close interdisciplinary cooperation between medicine, engineering, industry, and computer science. He has spent several research leaves as a Visiting Assistant Professor with the Brigham and Women's Hospital, Harvard Medical School. He is motivated by a number of challenging problems in medical image analysis. One important issue he is currently researching is the segmentation, modeling, and morphometric analysis of structures extracted from 3-D image data and 3-D time series obtained from medical imaging. His current focus is on shape-based 3-D object representation for automated object extraction and shape analysis of brain structures for studying neurodevelopmental and neurodegenerative changes in the human brain. His clinical applications include magnetic resonance imaging (MRI) studies in neonatal development, and studies of schizophrenia, autism, and depression. He is a member of the Editorial Board of the journal *Medical Image Analysis*, which is published by Elsevier.

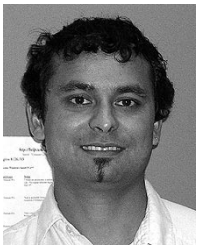

Sarang Joshi received the B.S. and D.Sc. degrees from Washington University, St. Louis, MO, in 1990 and 1998, respectively, both in electrical engineering.

He is currently an Assistant Professor with the Departments of Radiation Oncology and Biomedical Engineering, and an Adjunct Assistant Professor with the Department of Computer Science, University of North Carolina (UNC), Chapel Hill. His research interests include computational anatomy, statistics, pattern theory, adaptive radiation therapy, and four-dimensional (4-D) radiation treatment planning.

Stephen R. Aylward (Associate Member, IEEE) received the B.S. degree in computer science from Purdue University, West Lafayette, IN, in 1988, the M.S. degree in artificial intelligence from the Georgia Institute of Technology, Atlanta, in 1989, and the Ph.D. degree in medical image processing from the University of North Carolina, Chapel Hill, in 1997.

He is currently the Director of the Computer-Aided Diagnosis and Display Laboratory, Radiology Department, University of North Carolina. He is an Associate Professor with the Department of Radiology and an Adjunct Associate Professor with the Departments of Surgery and Computer Science, University of North Carolina. He is a consultant to Medtronic and R2 Technologies. His research focuses on the development of the Insight Toolkit and segmenting and registering vasculature for minimally invasive vascular interventional and partial-organ transplant procedures.

Dr. Aylward is an Associate Editor for the IEEE TRANSACTIONS ON MEDICAL IMAGING.